Mon. Not. R. Astron. Soc. **290**, 680–688 (1997)

Evolution of the radio outburst from the supermassive star η Carinae from 1992 to 1996

R. A. Duncan,[1★] S. M. White[2★] and J. Lim[3★]

[1] *Australian Telescope National Facility, PO Box 76, Epping, NSW 2121, Australia*
[2] *Department of Astronomy, University of Maryland, College Park, MD 20742, USA*
[3] *Institute of Astronomy and Astrophysics, Academia Sinica, PO Box 1–87, Nankang, Taipei, Taiwan 115, Taiwan*

Accepted 1997 June 17. Received 1997 June 2; in original form 1997 April 22

ABSTRACT

An earlier paper, describing observations at a wavelength of 3 cm with the Australia Telescope Compact Array between 1992 June and 1994 May, showed the supermassive star η Carinae to be in the throes of a major outburst. This paper, based on observations at wavelengths of both 3 and 6 cm, describes the evolution of the outburst since 1994 May.

From 1994 May to 1995 December, η Carinae's image continued to expand, and its total flux density to increase. These dramatic changes were caused, we believe, by an outburst of UV luminosity, and consequent ionization of pre-existing circumstellar gas clouds. Since 1995 December, η Carinae's total flux density has fallen.

The large-scale structure of the radio image closely resembles Hα optical images of the η Carinae 'Homunculus' nebula. In addition, the central area shows fine-scale structure, principally comprising a secondary source about 1.2 arcsec to the north-west of the star, which we believe to be a dense gas cloud, and a ridge of length 4 arcsec centred on the optical position of the star, which we believe to be an equatorial disc or torus. These structures are seen also in 3-cm (H91α) recombination-line emission.

Key words: stars: activity – stars: individual: η Carinae – supergiants – H II regions – radio continuum: stars – radio lines: stars.

1 INTRODUCTION

With a mass variously estimated between 100 and 150 $M_\odot$ (Meaburn et al. 1983; van Genderen & Thé 1984), η Carinae is thought to be the most massive star in the Galaxy, and has long been famous for its variability and nova-like mass ejections. An outburst beginning in the 1830s (Innes 1903; Gratton 1963; Walborn & Liller 1977) raised its visual magnitude to -1, making it for 15 yr the second brightest star in the sky. Subsequently, it dimmed to its present-day visual magnitude of 7. This dimming has been mainly caused by a resultant dust envelope and consequent conversion of its immense visual and UV energy to infrared. η Carinae has a current bolometric luminosity of 6×10^6 $L_\odot$ (Westphal & Neugebauer 1969), making it at 10 and 20 μm the brightest infrared source in the sky outside the Solar system (Neugebauer & Westphal 1968; Robinson, Hyland & Thomas 1973; Aitken & Jones 1975).

Observations of η Carinae between 1992 June and 1994 May with the Australia Telescope Compact Array (ATCA) at a wavelength of 3 cm (White et al. 1994; Duncan et al. 1995) showed η Carinae to be in the throes of a radio outburst; the flux density almost tripled in the period, and many new morphological features appeared. Since then, ATCA has monitored η Carinae's 3-cm continuum and hydrogen recombination-like emission at about 4-monthly intervals. Some of these observations have, in addition, included observations at 6 cm. This paper describes these more recent observations, and reports on the progress of the outburst.

★E-mail: rduncan@atnf.csiro.au (RAD); white@astro.umd.edu (SMW); jlim@biaa11.biaa.sinica.edu.tw (JL).

2 OBSERVATIONS

ATCA routinely observes simultaneously at two wavelengths. In the early observations, to double-check the results, we usually observed at two adjacent but independent 3-cm wavelengths. More recently, with confidence established, we usually observed at 3- and 6-cm wavelengths. One of the 3-cm wavelengths was usually centred on the H91α hydrogen recombination line, and the 6-cm wavelength was always centred on the H106α recombination line.

Except in an early pilot study in 1992 April, the configuration used comprised six 22-m antennas placed along a 6-km east–west array such that the baselines were almost equally spaced from 337 to 5939 m. At an observing wavelength of approximately 3 cm, this set of baselines was insensitive to structure larger than about 30 arcsec and so resolved out the general Carinae nebula, but imaged structure close to η Carinae with a nominal resolution of about 1 arcsec. In practice, because of the excellent signal-to-noise ratio, use of the 'MEM' algorithm (Narayan & Nityananda 1986; Cornwall & Braun 1989) yielded an actual resolution of about 0.5 arcsec. Similarly, at a wavelength of 6 cm it yielded an actual resolution of about 1 arcsec.

Table 1. Observing parameters.

Date	1st Frequency (MHz)	2nd Frequency (MHz)	Band-width (MHz)	No. Channels
92 Apr 29	8256	9024	128	32
92 Jun 29	8128	9024	128	32
93 Jun 18	8585 (H91α)	8873 (H90α)	64	64
94 Jan 30	8585 (H91α)	8730	128	64
94 May 1	8585 (H91α)	–	128	64
94 May 3	8585 (H91α)	8500	128	64
94 Sep 5	8585 (H91α)	5444 (H106α)	128	64
95 Jan 4	8585 (H91α)	8873 (H90α)	128	64
95 Apr 11	8585 (H91α)	8873 (H90α)	128	64
95 Nov 9	8585 (H91α)	5444 (H106α)	128	64
95 Dec 10	8585 (H91α)	5444 (H106α)	128	64
96 Apr 2	8585 (H91α)	5444 (H106α)	128	64
96 Jul 18	8585 (H91α)	5444 (H106α)	128	64
96 Oct 7	8585 (H91α)	5444 (H106α)	128	64

We used the standard Australia Telescope calibrator, PKS B1934 – 638, which is assumed to have a flux of 5.026 Jy at 5444 MHz and 2.864 Jy at 8585 MHz (Reynolds 1995), to calibrate all fluxes.

Table 1 gives details of the observing dates, frequencies, and other parameters. All but the 1993 June spectral-line observations were made with a bandwidth of 128 MHz, which yielded a useable velocity range of about ± 1700 km s^{-1} for the H91α (3-cm) recombination line, and ± 3400 km s^{-1} for the H106α (6-cm) line.

The frequent observing sessions (Table 1) allowed almost all results to be repeatedly confirmed. This paper uses observations made at the peak of the outburst (1995 December; see Fig. 2) to illustrate the H91α recombination-line spectra and source structure, but slightly later observations (1996 April) to illustrate the continuum emission. In April, because η Carinae then transited close to midnight, atmospheric stability, and consequent dynamic range, were superior.

Images and spectra were obtained by using AIPS and MIRIAD software packages.

3 RESULTS

3.1 Evolution of the continuum image

As reported earlier (Duncan et al. 1995), between 1992 June and 1994 May, the radio image at 3 cm grew from a single quasi-stellar source with an integrated continuum flux of 0.8 Jy (White et al. 1994) to a complex but approximately double source with an integrated flux of 2.2 Jy. [The initial, 1992 June, observation, though yielding accurate flux and morphology, because of the poor array calibration of the then newly commissioned telescope, gave an unreliable position (White et al. 1991).]

After 1994 January, changes in the image morphology, although less dramatic than those occurring earlier (Duncan et al. 1995), none the less continued. The initial symmetrical source seen in 1992 June, corresponding, we believe, to the star, continued to elongate and finally became a NE–SW ridge with a length exceeding 4 arcsec (Fig. 3). Fig. 1 illustrates this: it shows the images in 1994 January and 1995 December respectively, and the differ-

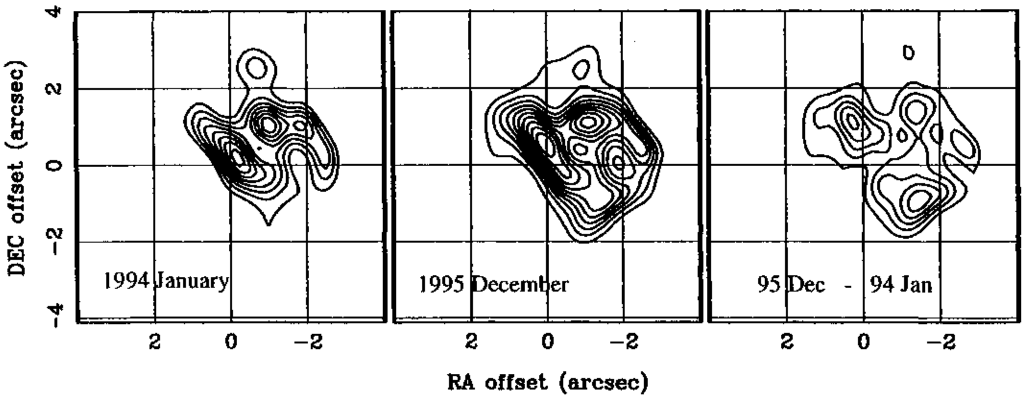

Figure 1. Continuum images of η Carinae at a wavelength of 3 cm (8585 MHz) in 1994 January (left) and 1995 December (centre), and the difference between these two images (right). Here, and in all image figures, image coordinates are relative to Davidson's optical position of the star, i.e., RA $10^h45^m03\overset{s}{.}615$, Dec. $-59°41'03\overset{''}{.}96$. Lowest contour 50 mJy arcsec^{-2}; contour interval 50 mJy arcsec^{-2}.

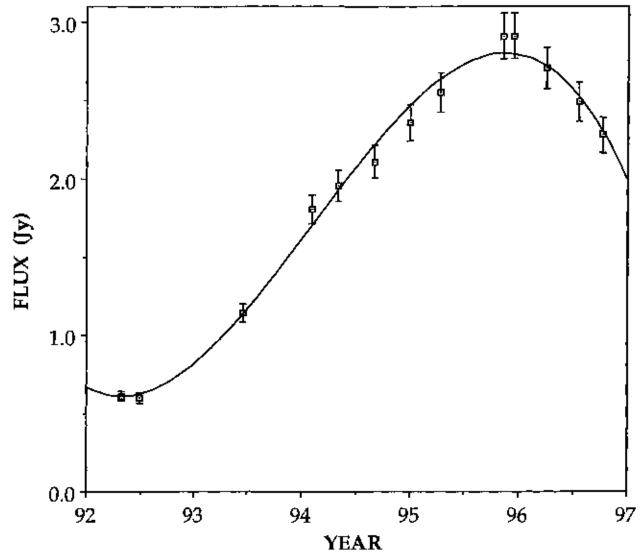

Figure 2. The evolution, over a 5-yr period, of η Carinae's 8585-MHz flux density. Error bars are ± 5 per cent.

ence between these two images. As we see, the original or central component had already grown somewhat ridge-like by 1994 January, and as the difference image shows, it subsequently continued to grow mainly at its north-east and south-west ends, i.e., to elongate and become even more ridge-like.

Fig. 2 shows the evolution of the total flux from 1992 April until 1996 October. Because η Carinae is variable in both flux and morphology, there is no quantitative method of estimating the probable error of an individual flux measurement. However, if extreme care is taken, flux measurements of non-variable sources are repeatable to within about 1 per cent (J. E. Reynolds, private communication), and experience suggests that under routine conditions error limits of about 2 or 3 per cent are attained. In Fig. 2 we have been conservative and drawn error bars of ± 5 per cent. As one can see from Fig. 2, the flux increased monotonically until 1995 November and December, then reaching 2.8 Jy, and thereafter declined.

Because 6-cm imaging observations have been made on only six occasions (Table 1), the evolution of the 6-cm flux and image morphology are less well determined.

3.2 3- and 6-cm continuum image morphology

Fig. 3 shows the 3-cm-wavelength (top) and the 6-cm-wavelength (bottom) continuum images observed in 1996 April.

Although it can be seen equally well in 3-cm images if their brightness sensitivity is increased by Gaussian convolution to a larger beamwidth, in Fig. 3 the large-scale morphology is best seen in the 6-cm-wavelength image. This large-scale structure closely resembles Hα and N II optical images of η Carinae (NASA 1994; Currie et al. 1996). The large SE–NW trending oval structure with a major axis of about 15 arcsec corresponds to the optical 'Homunculus'. The isolated region 12 arcsec south-west of the map centre corresponds to the optical south-west shell.

In addition, in the central region, within about ± 3 arcsec of the star, the radio images show fine-scale structure. Although it can be recognized in the 6-cm image, this fine-scale structure is seen with better resolution in the 3-cm image. Its main components are a NE–SW trending ridge with a length slightly exceeding 4 arcsec centred close to the optical position of the star (K. Davidson, private communication), and a smaller more symmetrical source about 1.2 arcsec to the north-west. In the 6-cm image, the central NE–SW ridge looks like a torus, and resembles a feature of the 10.2- and 11.2-μm infrared images observed by Hyland et al. (1979).

3.3 Spectral indices

A comparison of the 3- and 6-cm images enables one to deduce the emission's spectral index (α), here defined as

$$\alpha = (\log F_1 - \log F_2)/(\log \nu_1 - \log \nu_2),$$

where the 'F's are the observed fluxes, and the 'ν's are the corresponding observing frequencies. Before doing this, one must convolve the beamwidth of the 3-cm image up to that of the 6-cm image, and because beamwidth is poorly defined in an MEM image, we have based our spectral index map (Fig. 4), not on the images in Fig. 3, but on lower resolution Högbom-CLEAN images.

As Fig. 4 shows, the spectral index is greatest (1.8) at the centre of the source and decreases steadily outwards. Fig. 4 omits the outer Homunculus and south-west shell, because in faint regions the index derived from individual pixels is noisy. None the less, if one bears in mind that the third lowest brightness contour in the 6-cm image corresponds to the lowest contour in the 3-cm image, one may visually compare the 6- and 3-cm brightnesses in Fig. 3, and this comparison shows the index in these faint outer regions to be zero or marginally negative.

3.4 H106α (6-cm) spectral emission

On the first occasion on which we observed in the H106α band (1994 September 5; Table 1), weak H106α emission was detected (Fig. 5). The H106α spectral peak has a height of only 3.2 mJy, a little more than twice the noise, but the fact that the phase is close to zero over the width of the peak suggests that the peak is real.

During five subsequent observing sessions in this frequency band (all more than a year later; Table 1) no H106α (6-cm) hydrogen recombination-line emission was detected. The main conclusion must be that H106α emission is weak and usually undetectable.

3.5 H91α (3-cm) spectral emission

The H91α (3-cm) hydrogen recombination-line emission observed between 1993 June and 1994 May has been described by Duncan et al. (1995). When first observed in 1993 June the spectral peaks were narrower than at present, and consequently the two components described later were completely separated. Subsequently, however, from 1994 January to 1995 December, although its amplitude almost doubled, the profile of the H91α spectrum (excepting the wings) remained remarkably constant. Fig. 6 shows the

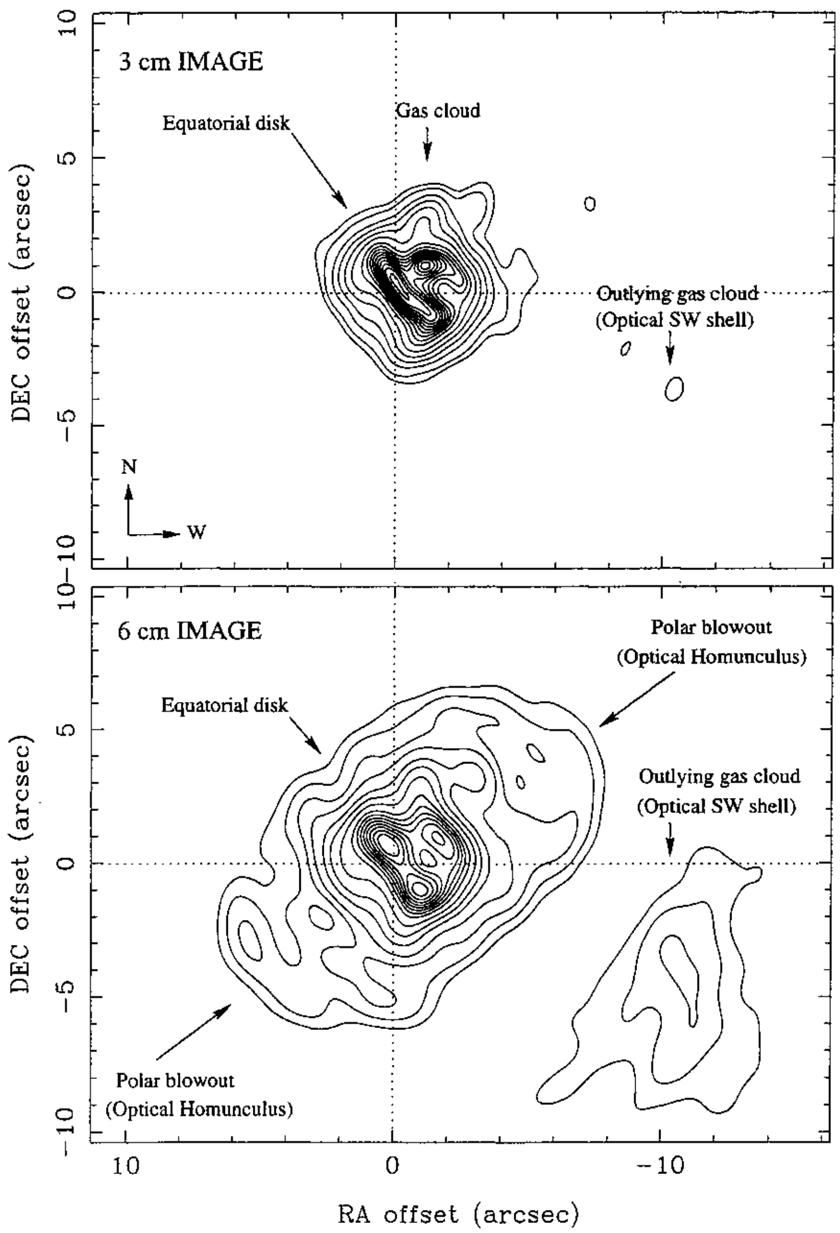

Figure 3. Continuum images of η Carinae at wavelengths of 3 cm (top) and 6 cm (bottom) respectively, as observed in 1996 April. Image centres as in Fig. 1. Contour brightness levels, in units of mJy arcsec^{-2}: 3-cm: 1, 2, 5, 10, 20, 40, 80, 120, 160, 200, 240, 280, 320, 360, 400 and 440. 6-cm: 0.25, 0.5, 1, 2, 5, 10, 20, 40, 60, 80, 100, 120, 140, 160, 180, 200, 220 and 240.

H91α recombination-line spectrum observed in 1995 December, the month when the outburst reached its maximum. This spectrum shows the integrated flux over a large (5×10 arcsec^2) inclined rectangle covering the spectral-emitting region (see Fig. 7). The spectrum shows a peak of width ± 250 km s^{-1} centred at -286 km s^{-1}. This great width is, we believe, the largest ever observed from circumstellar matter (cf. Subrahmanyan et al. 1993).

Fig. 7 is the corresponding spectral image cube. (The velocities on each panel are simply channel-centre velocities; our velocity resolution is only 70 km s^{-1}.) It shows that the strongest emission, corresponding to the spectral peak (-286 km s^{-1}), arises from a position 1.2 arcsec north-west of the map centre, i.e., the position of the new continuum source which first appeared in 1993 June (Fig. 3). In addition, weaker, broader and, on the whole, redder emission arises from a ridge spreading north-east and south-west of this position, corresponding to the NE–SW ridge seen in the continuum emission (Fig. 3).

Fig. 8 shows two spectra based, respectively, on emission arising from these two regions. The first spectrum is that of emission arising within an 0.5×0.5 arcsec^2 box centred 1 arcsec north and 1.2 arcsec west of the map centre; this corresponds to the position of the dominant source in the -286 km s^{-1} frame of Fig. 7, and to the north-west source in the continuum image (Fig. 3). The second spectrum is that of the average emission arising in two 0.5×0.5 arcsec^2 boxes, one centred 1.5 arcsec north and 0.4 arcsec east of

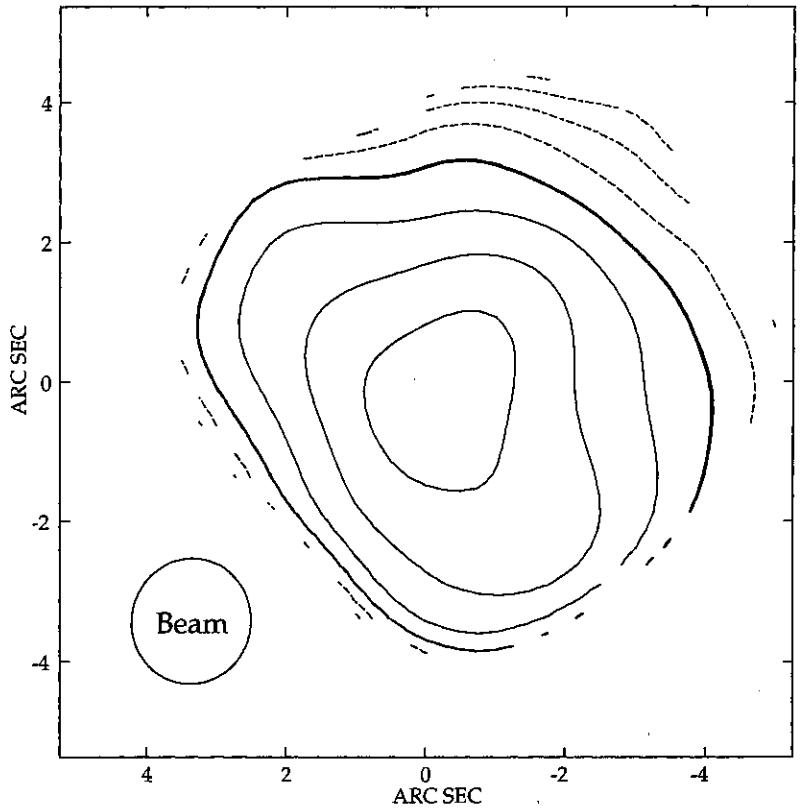

Figure 4. Spectral index map of η Carinae. Map centre as in Fig. 1. Broken contours negative, heavy contour zero, solid contours positive. Contour intervals 0.5.

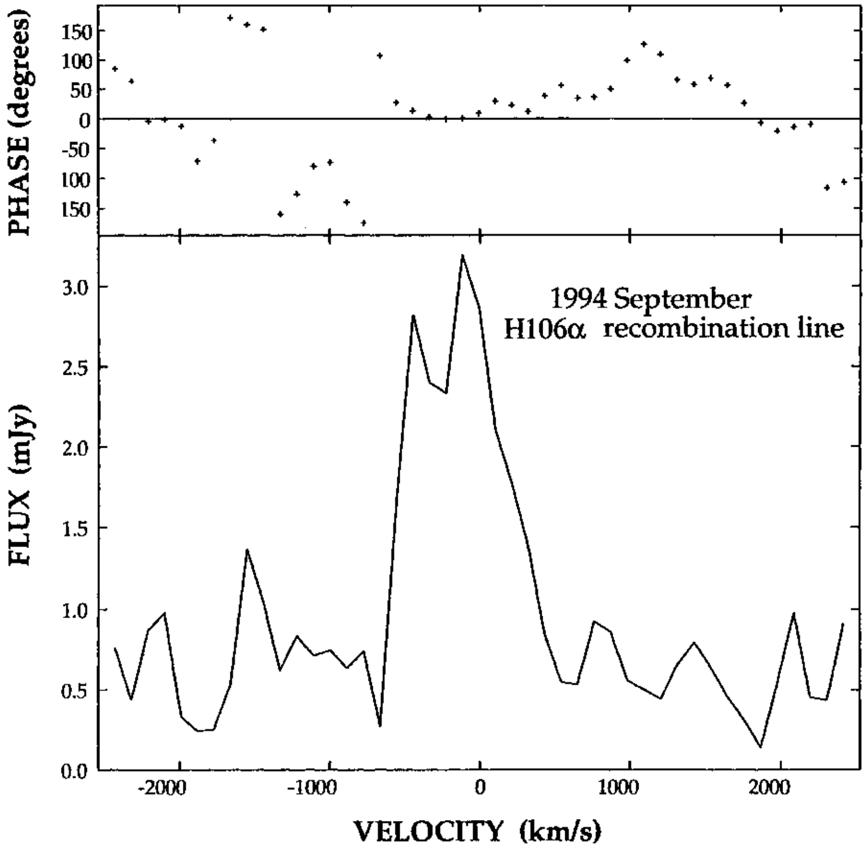

Figure 5. H106α (6-cm) hydrogen recombination-line spectrum observed in 1994 September.

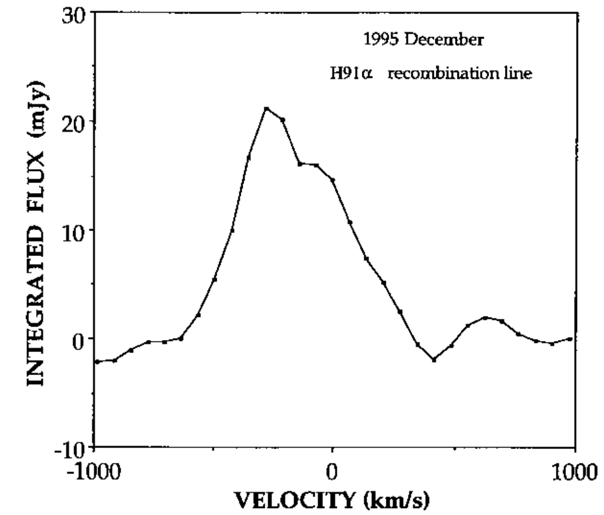

Figure 6. H91α (3-cm) hydrogen recombination-line spectrum observed in 1995 December. The integrated spectral flux over a 5×10 arcsec^2 inclined rectangle covering the spectral emitting region (see Fig. 7).

the map centre corresponding to the north-east subpeak in the -5 km s^{-1} frame of Fig. 7, and the other centred 0.4 arcsec south and 1.5 arcsec west of the map centre corresponding to the south-west subpeak in the -5 km s^{-1} frame of Fig. 7. Together these represent the NE–SW torus seen in both Figs 3 and 7 (as explained in the next section, we take the two ends of the NE–SW band seen in Fig. 7 to represent the torus, because the central part receives its main contribution from the north-west source). Although spectra from both the north-west source and the NE–SW torus are broad, that from the NE–SW torus is by far the broader.

The strength of the recombination emissions from the north-west source has varied only slowly during the history of the outburst. For example, comparison of the -285 km s^{-1} frames of the spectral cubes for 1995 December (Fig. 7) and 1996 April (not shown) reveals that the only difference between the dominant (north-west) sources in the two sessions is that the 1996 April source lacks the abrupt cut-off (i.e., very close contours) seen on the north-west side of the source in the 95 December image, and is thus more symmetrical. Possibly this cut-off is artificial and the result of a shorter observing session and consequently poorer beam-shape in 1995 December. Except for this minor point, emissions from the north-west source in the two sessions were identical.

In contrast, the NE–SW torus has varied rapidly; in 1996 April emission from the torus was very much weaker than in 1995 December, and this decline was undoubtedly real.

Fig. 9 shows, for the -75 km s^{-1} frame, the difference between the 1995 December and 1996 April recombination emissions, and quantifies the behaviour described above. Because of the north-west source's great strength and the small change described above, it has not been completely eliminated by this subtraction (it instead appears as negative contours at its north-west edge), but it has been almost eliminated, thus showing that it was of practically equal strength in 1995 December and 1996 April. The NE–SW

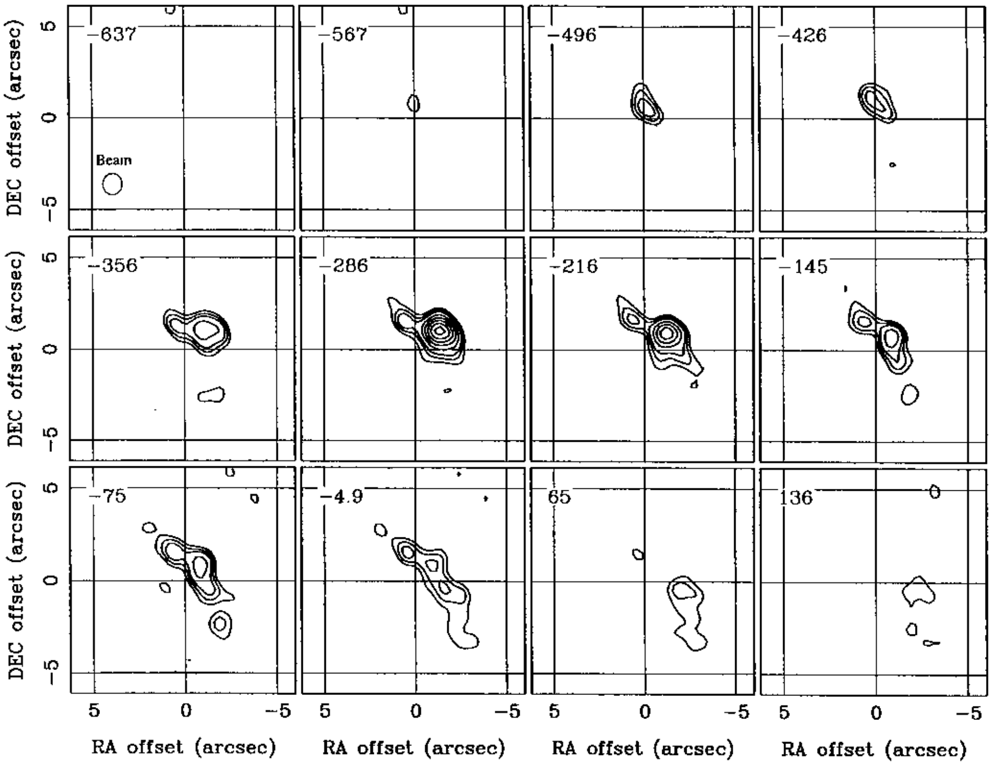

Figure 7. Images of H91α (3-cm) hydrogen-recombination line emission observed in 1995 December, for each of 12 adjacent velocity channels. The central velocity of each 70 km s^{-1} wide channel is given in each image. Contour brightness levels: 1.5, 2.0, 2.5, 3.5, 4.5, 5.5, 6.5 and 7.5 mJy arcsec^{-2}.

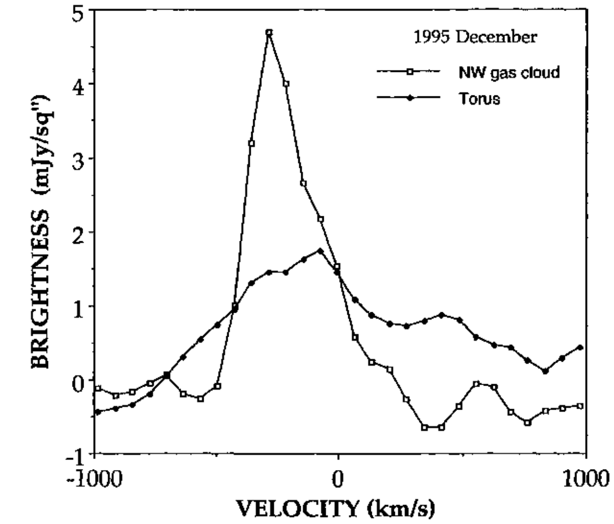

Figure 8. H91α (3-cm) hydrogen recombination-line spectra from each of two areas of the η Carinae image (see Figs 3 and 7): the north-west gas cloud, and the equatorial torus. The spectra were taken in 1995 December. See text for details.

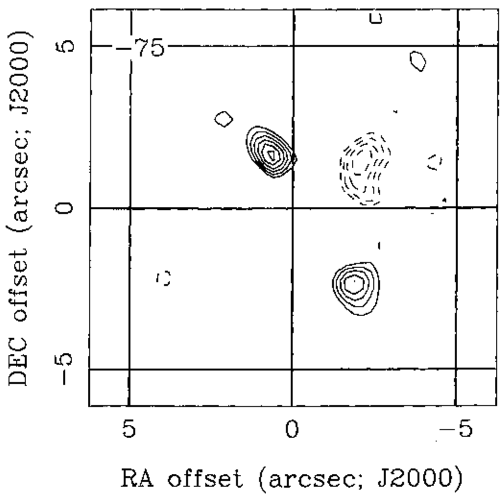

Figure 9. Difference between the -75 km s^{-1} velocity channel images of the H91α (3-cm) hydrogen-recombination line emission for 1995 December and 1996 April (December minus April). Image centre as in Fig. 1. Negative contours dashed, positive contours solid. Brightness of outermost ('lowest') contours ± 1.5 mJy arcsec^{-2}, contour intervals 0.25 mJy arcsec^{-2}.

torus, by contrast, despite its relative weakness in the original images, stands out clearly in the difference image (Fig. 9), showing that it was much stronger in 1995 December than in 1996 April.

4 DISCUSSION

4.1 Overview of recent radio outburst

In 1992 June, at a wavelength of 3 cm, η Carinae appeared as a strong central quasi-stellar source, surrounded by a weak halo corresponding to the inner half of the optical Homunculus (White et al. 1994). (Although it was not reported at the time, we also detected emission coinciding with the optical south-west shell.) The central emission lacked polarization and had a rising spectral index, and we therefore associated it with the star, and concluded that, as suggested by Davidson (1971), the emission arose as thermal bremsstrahlung in a dense stellar wind. In subsequent months and years the 3-cm radio emission in the innermost ± 4 arcsec brightened, and the source structure grew more complex. The main changes were the lengthening of the original quasi-stellar source into a ridge, the advent of a new source about 1.2 arcsec north-west of the image centre, and general brightening (Fig. 2).

We ascribed the new source components and the general brightening to the excitation of pre-existing circumstellar gas by a disturbance propagating from the star (Duncan et al. 1995). The only plausible disturbance capable of travelling with the implied minimum velocity of 50 000 km s^{-1} is electromagnetic radiation, and we therefore attributed the observed changes to the ionization of pre-existing neutral gas by a stellar outburst of UV radiation.

The observations reported here provide no reason to change this basic model. However, the continued growth of the radio flux till 1995 December increases our estimate of the additional ionizing UV flux to $10^{48.1}$ photon s^{-1}, and our estimate of the minimum additional ionized mass to 0.06 $M_{\odot}$. In addition, our improved data enable us to identify more confidently the source components.

4.2 Morphology

As we have said, the 6-cm radio image (Fig. 3, bottom) closely resembles optical images (e.g. NASA 1994; Duschl et al. 1995; Currie et al. 1966) of η Carinae. The large-scale oval, trending SE–NW with a major axis of about 15 arcsec, corresponds to the optical 'Homunculus'. Opinions have oscillated over the years, but from the optical evidence we strongly agree with those who identify it with polar outflow (e.g. Duschl et al. 1995). From optical velocity measurements, Currie et al. (1966) have shown that almost all of this outflow originated in the single eruption of $\sim$1841.

The isolated source about 12 arcsec south-west of the map centre, seen also, though barely above the noise level, in the 3-cm image, coincides with an outlying optically well-known gas shell (NASA 1994). The optical Homunculus is known to have developed from gas ejected during the great outburst of the 1840s (van Genderen & Thé 1984; Currie et al. 1966), and velocity measurements suggest that this south-west shell comprises gas ejected in an earlier unrecorded outburst (Walborn, Blanco & Thackeray 1978).

The ridge-like structure near the map centre with a major axis of about 4 arcsec (best seen in the 3-cm images) has evolved from the simple quasi-stellar source observed in 1992 June (Fig. 1). This ridge is normal to the major axis of the supposed polar outflow (Fig. 3), and its centre is close to the optical position of the star (K. Davidson, private communication). For these reasons, and because of a similar feature in infrared (Hyland et al. 1979) and optical (Duschl et al. 1995; Currie et al. 1966) images, we believe it to be an equatorial torus.

Consequently, we believe the centre of this ridge to mark the position of the star. The optical position we have adopted as our map centre (RA $10^{h}45^{m}3^{s}.615$, Dec.

$-59°41'3''.96$) was measured at Cerro Tololo Inter-American Observatory in about 1989 (K. Davidson, private communication). Our radio images (Figs 2 and 3) suggest a position of about 0.4 s in RA west of that, i.e, a position RA $10^h45^m03^s.22$, Dec. $-59°41'4''.0$.

We have already argued that the small source about 1.2 arcsec north-west of the map centre (best seen in the 3-cm image) is a circumstellar gas cloud (Duncan et al. 1995). An unexplained characteristic of this source is its slight elongation (Fig. 1) or tail (Fig. 3, top), along an axis parallel to that of the central ridge. None the less, we maintain belief that it is a gas cloud.

4.3 Spectral index

Close to the map centre (even with our low resolution) the spectral index reaches 1.8 (Fig. 4), and this high value implies that the gas close to the map centre is sharply bounded and almost optically thick to radio emission (Mezger, Schraml & Terzian 1967; Panagia & Felli 1975; Wright & Barlow 1975).

Furthermore, the four or so years taken for the inner gas clouds to reach their maximum degree of ionization implies great optical thickness to UV radiation. None the less, the fact that the outer Homunculus and south-west shell are ionized shows that some UV radiation escapes, and to reconcile this escape with large UV optical thickness we must conclude that the inner gas distribution is clumpy. Also, if, as we have argued, much of the innermost gas lies in the form of a disc or torus, this will enable UV propagating away from the plane of the torus to escape. Optical images (e.g. Duschl et al. 1995) suggest that even within the torus the gas distribution is clumpy.

The observed decrease of spectral index with increasing distance from the star (Fig. 4) implies, as it to be expected, decreasing radio optical-depth, i.e., decreasing electron density, with increasing distance from the star.

In a small area about 4 arcsec north-west of the star the spectral index apparently becomes negative (Fig. 4). Because of the possibility of an 'edge effect' arising from a residual inaccuracy in convolving the 3- and 6-cm images to the same effective beamsize, one should accept this evidence with caution, but if it were true it would suggest that non-thermal shock emission occurs in this area. It is perhaps relevant that Currie et al. (1966), although finding that most gas motion in the neighbourhood of η Carinae was orderly, and consistent with a single ejection in $\approx$1841, also found anomalously high gas velocities at the north-west edge of the Homunculus. Gas with much higher velocities than that of the general Homunculus could well cause non-thermal shocks.

However, as we have said, over most of the outer regions (the Homunculus and south-west shell) comparison of the 3- and 6-cm continuum images (Fig. 3) shows the spectral index to be zero or marginally negative, and this is completely consistent with optically thin thermal emission (Mezger et al. 1967).

4.1 H106α (6-cm) spectral emission

H106α (6-cm) spectral emission was detected only during the first (1994 September) of the six observing sessions during which it was sought, and even then was weak. One expects weaker recombination-line emission at longer wavelengths (Kardashev 1960), and the high gas density in the inner regions, as revealed by the continuum spectral index, probably disfavours recombination-line emission at the longer (6-cm) wavelength even further (Aller 1984).

4.5 H91α spectral emission

H91α recombination-line emission was detected only in the bright central region of the continuum image (cf. Figs 3 and 7). As our detection threshold for spectral emission was relatively high, 3 mJy, this is not surprising. The H91α spectrum has two components: extremely broad emission centred at a velocity of approximately -75 km s^{-1}, and relatively narrow (but still broad) emission centred at a velocity of approximately -250 km s^{-1} (Fig. 8). In 1993 June (Duncan et al. 1995) both spectral components were much narrower, suggesting that in that early stage of the outburst both gas temperature and turbulence were lower.

Figs 7 and 8, together, show that these two components arose from different positions in the sky; the image cube (Fig. 7) illustrates this in greatest detail. Although each frame has contributions from both spectral components, the -286 km s^{-1} frame is dominated by the narrower spectral component, and frames progressively further away from this -286 km s^{-1} frame (e.g., the -5 km s^{-1} frame) become increasingly free of this domination and more representative of the extremely broad component.

The narrower spectral component (Fig. 7: the -286 km s^{-1} frame) arises 1.2 arcsec north-west of the image centre, i.e., it arises from the position of the continuum source which first appeared in 1993 June (Fig. 3). We have already argued that this north-western continuum source arises from a dense, newly ionized gas cloud close to the star, and we must conclude that the narrower component of H91α emission arises from the same cloud. Theory shows that the ratio of spectral-line to continuum brightness increases with decreasing temperature (Kardashev 1960), and hence the cloud's brighter H91α emission suggests that, as one would expect, it is cooler than the stellar torus. Its width and central velocity of about -250 km s^{-1} show, respectively, that it is turbulent and moving rapidly towards us.

As we have said, the -75 and -5 km s^{-1} frames of Fig. 7 are dominated by the extremely broad spectral component. The elongated NE–SW running sources in these frames are slightly arched towards the north-west. We believe that this is because of residual contamination by the strong north-west source (see the -286 km s^{-1} frame), so that to obtain minimally contaminated positions and orientations of these NE–SW ridges one should draw straight lines between their extremities. If, for example, one does this in the -75 km s^{-1} frame, and takes the pinched-off contours at each end to be the extremities, then the joining line has an orientation (38° east of north) and position identical with the feature in the continuum image (fig. 3) which we have identified as an equatorial torus. Perhaps the easiest way to demonstrate this is to overlay either Fig. 9, or the -75 or -5 km s^{-1} frames in Fig. 7, on Fig. 3. In both continuum (Fig. 1) and H91α line emission (Duncan et al. 1995) this feature was fairly symmetrical in earlier years, but has since grown ridge-like. Its low average velocity is consistent with its being closely associated with the star. We therefore suggest that, like the ridge-like continuum feature, the extremely broad spectral emission arises from gas in a stellar torus.

4.6 Electron temperature

The peak continuum brightness, and hence the brightness temperature (T_b) deduced from it, depends on the resolution of the image; poorer resolution smears the flux over a larger area and lowers the apparent temperature. The peak brightnesses shown in the high-resolution MEM images for the peak of the outburst, 1995 December (analogous to Fig. 3), imply a peak temperature of 8000 K at a wavelength of 3 cm, and 11 000 K at a wavelength of 6 cm. (It should be noted in passing that the 3- and 6-cm peaks occur at slightly different positions of the images, and hence cannot be used to deduce a spectral index.) If the structure is resolved, and if, as we believe, the region is very close to optically thick at 6-cm wavelength, the 6-cm value will equal the electron temperature (T_e); otherwise it will be lower limit.

Alternatively, the electron temperature (T_e) can be estimated from the ratio of line to continuum emission by using expressions 2.121 and 2.122 in Lang's 'Astrophysical Formulae' (1980). Using the value for the peak 3-cm continuum brightness for 1995 December, and the line brightness given in Fig. 8, we obtain electron temperatures (T_e) of 5000 K in the north-west cloud, and 6000 K in the torus. These estimates are lower than that deduced from the 3-cm continuum brightness (8000 K), and there are at least two possible reasons for this discrepancy. Lang's formulae assume local thermodynamic equilibrium (LTE), and although most departures from LTE enhance rather than decrease such estimates of electron temperature (Lang 1980), the disagreement perhaps suggests that the plasma is not in LTE. Another possible source of error is that our spatial resolution is higher in the continuum than in the spectral data. Hence the estimate based on the 6-cm continuum brightness, 11 000 K, is probably the most reliable.

4.7 Summary

In summary, therefore, radio images of η Carinae show three main features. The first is a large-scale ($\sim$15-arcsec) oval seen in continuum, coincident with the optical Homunculus, and which we believe comprises polar blowout. The second is a small ($\sim$4 arcsec) ridge seen in both continuum and recombination-line emission, which is at the centre of, and normal to, the major axis of the Homunculus, and which we believe to be a stellar equatorial torus. The third is a small symmetrical source 1.2 arcsec north-west of the star, seen in both continuum and recombination-line emission, which we believe to be an isolated dense gas cloud.

ACKNOWLEDGMENT

We are greatly indebted to Dr James Caswell for advice during the preparation of this paper.

REFERENCES

Aitken D. K., Jones B., 1975, MNRAS, 172, 141
Aller L. H., 1984, Physics of Thermal Gaseous Nebulae. Reidel, Dordrecht, p. 96
Cornwall T., Braun R., 1989, in Perley R. A., Schwab F. R., Bridle A. H., eds, ASP Conf. Ser. Vol. 6, Synthesis Imaging in Radio Astronomy. Astron. Soc. Pac., San Francisco, p. 167
Currie D. G., Dowling D. M., Shaya E. J., Hester J. J., Scowen P., Groth E. J., Lynds R., O'Neil E. J., 1996, AJ, 112, 1115
Davidson K., 1971, MNRAS, 154, 415
Duncan R. A., White S. M., Lim J., Nelson G. J., Drake S. A., Kundu M. R., 1995, ApJ, 441, L73
Duschl W. J., Hoffmann K.-H., Rigaut F., Weigelt G., 1995, Rev. Mex. Astron. Astrofis., 2, 17
Gratton L., 1963, Star Evolution. Academic Press, New York, p. 297
Hyland A. R., Robinson G., Mitchell R. M., Thomas J. A., Becklin E. E., 1979, ApJ, 233, 145
Innes R. T. A., 1903, Cape Obs. Ann., 8, 75B
Kardashev N. S., 1960, AJ, 3, 813 (English translation)
Lang K. R., 1980, Astrophysical Formulae. Springer-Verlag, Berlin
Meaburn J., Walsh J. R., Hebden J. C., Morgan B. L., Vine H., 1983, MNRAS, 204, 41P
Mezger P. G., Schraml J., Terzian Y., 1967, ApJ, 150, 807
Narayan R., Nityananda R., 1986, ARA&A, 24, 127
NASA, 1994 Public domain computer file: pubinfo.jpl.nasa.gov/images/wfpc-06.gif
Neugebauer G., Westphal J. A., 1968, ApJ, 152, L89
Panagia N., Felli M., 1975, A&A, 39, 1
Reynolds J. E., 1995, ATNF Web site, http://wwwnar.atnf.csiro.au/observing/users-guide
Robinson G., Hyland A. R., Thomas J. A., 1973, MNRAS, 161, 281
Subrahmanyan R., Ekers R. D., Wilson W. E., Goss W. M., Allen D. A., 1993, MNRAS, 263, 868
van Genderen A. M., Thé P. S., 1984, Space Sci. Rev., 39, 317
Walborn N. R., Liller M., 1977, ApJ, 211, 181
Walborn N. R., Blanco B. M., Thackeray A. D., 1978, ApJ, 219, 498
Westphal J. A., Neugebauer G., 1969, ApJ, 156, L45
White S. M., Duncan R. A., Lim J., Nelson G. J., Drake S. A., Kundu M. R., 1994, ApJ, 429, 380
Wright A. E., Barlow M. J., 1975, MNRAS, 170, 41